SCIENCE CHINA
Technological Sciences

July 2012 Vol.55 No.7: 1886–1893
doi: 10.1007/s11431-012-4847-0

Achieving maximum power transfer of inductively coupled wireless power transfer system based on dynamic tuning control

QIANG Hao[1,2], HUANG XueLiang[1*], TAN LinLin[1], JI QingJing[1] & ZHAO JiaMing[1]

[1] *School of Electrical Engineering, Southeast University, Nanjing 210096, China;*
[2] *School of Information Science and Engineering, Changzhou University, Changzhou 213164, China*

Received July 25, 2011; accepted March 12, 2012; published online May 28, 2012

As an emerging research field, inductively coupled wireless power transfer (ICWPT) technology has attracted wide spread attention recently. In this paper, the maximum power transfer performances of four basic topologies labeled as SS, SP, PS and PP are investigated. By modeling the equivalent circuits of these topologies in high frequency (HF), the primary resonance compensation capacitances for maximum power transfer capability are deduced. It is found that these capacitances fluctuate with load resistance change, which is disadvantageous to SP, PS and PP topologies and an obstacle to their practical applications as well. To solve this problem, a phase controlled inductor circuit is proposed. By adjusting the triggering angle, the real-time dynamic tuning control can be achieved to guarantee maximum power transfer. Finally, simulations and experiments show that the proposed method is of great effectiveness and reliability to solve the issue of resonance compensation capacitance fluctuation with load change and to guarantee the flexible applications of all topologies.

dynamic tuning, inductively coupled, topology, wireless power transfer

Citation: Qiang H, Huang X L, Tan L L, et al. Achieving maximum power transfer of inductively coupled wireless power transfer system based on dynamic tuning control. Sci China Tech Sci, 2012, 55: 1886–1893, doi: 10.1007/s11431-012-4847-0

1 Introduction

The traditional V-MODE is mainly based on the wired power supply, and there must be direct physical link between power and loads. Since Tesla had opened up the field of wireless power transfer (WPT) [1], WPT has been a dream for people. Over the years, various research activities have been carried out persistently by many scholars in this field [2–8], but with little progress achieved. It is not until 2007 that MIT made a new theoretical breakthrough on it, they used non-radiative electromagnetic energy resonant effect to successfully light up a 60W bulb 2 m away with about 40% transfer efficiency [9].

Inductive coupling and resonant coupling are two major means of the WPT technology. In either inductive or magnetic coupled systems, power is transferred from a primary transmitter coil to a secondary receiver coil with the aid of an alternating magnetic field.

The WPT technology quickly became a hot pursuing topic for research institutions in recent years [10–15], and some further breakthroughs have been made in electric vehicles, body implantable medical devices, small robots and portable mobile device chargers [16, 17]. To improve power transfer efficiency further, some scholars focused on changing the parameters of the resonator coils [18, 19] by increasing the radius of the conductor, or using multi-turn wire coils and so forth; other scholars attempted to study and design different resonance compensation topologies to achieve maximum transfer efficiency. In ref. [20], based on inductive coupling mode, Wang et al. analyzed the equivalent circuits and power

*Corresponding author (email: xlhuang@seu.edu.cn)

transfer capacity of various topologies, but their models are not precise enough due to the ignorance of parasitic parameters of coils in HF. In ref. [21], Zhou et al. studied the voltage and current gains of various topologies, but without the analysis of the condition of achieving maximum power transfer. Moreover, in ref. [22], Qiang et al. investigated and defined a condition criterion for the design of the appropriate topology to guarantee optimal transfer efficiency. It is shown that the design of the topology is correlated with some parameters like load, operating frequency and coil size. Different topologies should be designed to achieve the maximum transfer efficiency in different situations.

In this paper, in consideration of parasitic resistance and capacitance in HF, more precise equivalent circuit models of various topologies are set up. With the analysis of their maximum transfer capacity, the primary compensation capacitances of different topologies are deduced and these capacitances except that of SS topology are the functions of load resistance, i.e. these capacitances are not constant but fluctuate with load. In fact, as one power system, its load is of great randomness that the maximum transfer power and the system stability could not be guaranteed, which can be an obstacle to practical applications for other three topologies. To solve this problem, a phase controlled inductor circuit is further designed, with the aim of realizing real-time and dynamic tuning control to guarantee maximum power transfer and frequency stability by selecting the reasonable inductor circuit parameters and adjusting the triggering angle.

Through theoretical analysis and simulation experiments, the maximum energy transfer performances of different topologies of the inductively coupled wireless power transfer (ICWPT) system are studied, and a valid phase controlled inductor circuit is designed to tune the system real-timely and dynamically to guarantee the flexible application of the various topologies and lay the foundation for the next design of the WPT device. In Section 2, the models of the ICWPT system are set up in HF through equivalent circuit. In Section 3, the power transfer performances of four basic topologies are analyzed and the expressions of the primary resonance compensation capacitance deduced. A phase controlled inductor circuit is designed in Section 4 and the dynamic tuning controls are carried out for SP, PS and PP topologies respectively in Section 5. Finally in Section 6, the simulation and experimental results have verified the theoretical analysis and show that the proposed method is effective and reliable.

2 ICWPT system model

Through setting up the system physical model and building the internal equivalent parameters, the theoretical analysis is carried out in this paper. Figure 1 is a typical schematic diagram of the ICWPT system, which consists of two independent parts. The part connected to the power supply is called primary loop and the other part connected to load is called secondary loop respectively.

In addition to two coils for transferring power, the transmitting power source and receiving power device are indispensible for a complete ICWPT system. High frequency oscillation circuit and high frequency power amplifier are used to produce high frequency power source; L_P, L_S are two air core resonant coils (the subscripts "P" and "S" stand for the primary and secondary coils respectively); M and D are the mutual inductance and distance between the two coils. When the two coils are in self-resonant state and the resonance frequencies are consistent, the inductive power in L_S is transferred from L_P with maximum efficiency and powers the load R_L. Then the entire wireless transfer of power is completed.

To simplify the analysis, in this research only two transceiver coils, L_P and L_S, are equivalently studied. Using the standard mutual inductance coupling transformer model and assuming sinusoidal input voltage with the angular frequency ω, the induced voltage in the secondary coil due to the primary current (I_P) is equal to $j\omega MI_P$, while the reflected voltage in the primary coil due to the secondary current (I_S) is equal to $-j\omega MI_S$. The equivalent coupling circuit is shown in Figure 2.

3 Performance analysis of various resonance compensation topologies

Usually, in order to enhance the transfer efficiency, series or parallel compensation is applied in the primary or the secondary circuit. Four basic resonance compensation topologies labeled as SS, SP, PS and PP are shown in Figure 3, where the first S or P stands for series or parallel compensation of the primary circuit and the secondary S or P for series or parallel compensation of the secondary circuit.

Considering the fact that the system works in HF, the gen-

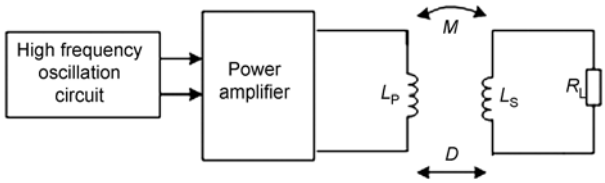

Figure 1 Schematic diagram of ICWPT system.

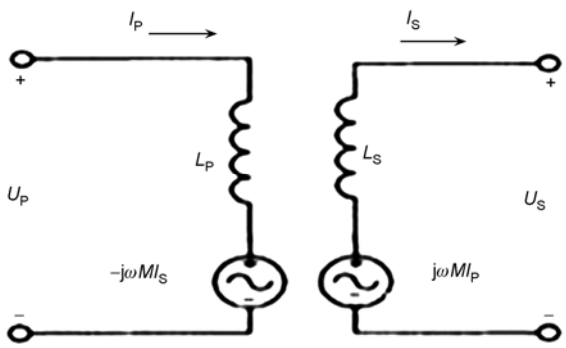

Figure 2 Equivalent circuit of WPT system.

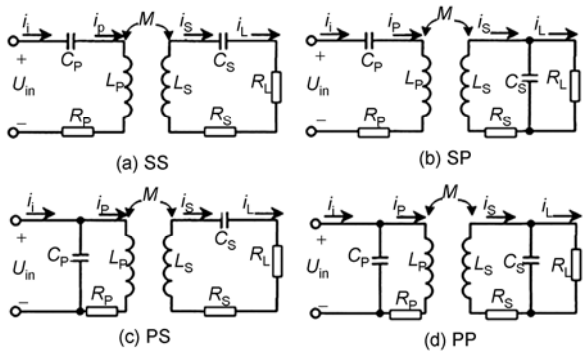

Figure 3 Four basic topologies.

erated parasitic parameters should not be ignored. In Figure 3, U_{in} stands for the induced potential source; R_P and R_S stand for the parasitic resistances of L_P and L_S respectively and the parasitic capacitances of two resonant coils are included in C_P and C_S; R_L stands for load resistance.

From Figure 2, it is easy to deduce the voltage KVL equations of the two circuits with the operating angular frequency ω.

$$\begin{cases} Z_P I_P - j\omega M I_S = U_P, \\ -j\omega M I_P + Z_S I_S = 0, \end{cases} \tag{1}$$

where Z_P and Z_S stand for the impedances of primary and secondary loops respectively. According to eq. (1), the equivalent currents of two coils can be obtained.

$$I_P = \frac{U_P}{Z_P + \dfrac{(\omega M)^2}{Z_S}}, \tag{2}$$

$$I_S = \frac{j\omega M \dfrac{U_{in}}{Z_P}}{Z_S + \dfrac{(\omega M)^2}{Z_P}}. \tag{3}$$

From eq. (2), the primary current (I_P) is correlated with Z_P and $(\omega M)^2/Z_S$. $(\omega M)^2/Z_S$ is referred to as the secondary-to-primary reflected impedance, describing the loading effect of the secondary circuit on the primary circuit, labeled as Z_{PS}. Similarly $(\omega M)^2/Z_P$ is the primary-to-secondary reflected impedance, labeled as Z_{SP}.

Then the power transferred from the primary coil to the secondary coil can be expressed as

$$P = (\mathrm{Re}\, Z_{PS}) I_P^2, \tag{4}$$

where Re represents the real component of the corresponding variable, while Im represents the imaginary component.

Theoretically, the receiving power of the secondary coil and the power transfer capability of the WPT system will be maximized if the system operates at the secondary resonance frequency as given by

$$\omega_0 = \frac{1}{\sqrt{L_S C_S}}. \tag{5}$$

Substituting eq. (5) into Z_{PS}, it is found that at angular frequency ω_0, Z_{PS} is pure resistance for series resonance secondary loop, whereas Z_{PS} is capacitive load for parallel resonance secondary loop.

After taking the reflected impedance Z_{PS} into account, the equivalent primary circuit is shown in Figure 4.

From Figure 4, the equivalent load impedance Z_{Peq} of the entire WPT system can be obtained and shown in Table 1.

In order to minimize the VA ratings of the power supply, it is desirable to operate at the zero phase angular frequency of the load impedance, which could be accomplished by adjusting C_P, and at the frequency the load reactance seen by the power supply is equal to zero, eliminating reactive power flow and increasing transfer power. Moreover, this zero phase angular frequency should be set at the secondary resonance frequency to maximize power transfer. To achieve this objective, the primary capacitance is selected to compensate both the primary self-inductance and the reflected impedance.

Solving $\mathrm{Im}Z_{Peq}(\omega=\omega_0)=0$, the primary compensation capacitances for the four basic topologies are calculated and shown in Table 2.

In Table 2, $\mathrm{Re}Z_{PS}$ and $\mathrm{Im}Z_{PS}$ represent the real and imaginary components of the reflected impedance for the parallel resonance secondary loop respectively, given as

$$\begin{aligned} \mathrm{Re}\, Z_{PS} &= \frac{(\omega_0 M)^2 (R_S (1 + \omega_0^2 C_S^2 R_L^2) + R_L)}{R_S^2 + 2R_S R_L + \omega_0^2 L_S^2}, \\ \mathrm{Im}\, Z_{PS} &= -\frac{\omega_0^3 M^2 L_S}{R_S^2 + 2R_S R_L + \omega_0^2 L_S^2}. \end{aligned} \tag{6}$$

As shown in Table 2, in SS topology, the designed primary resonance capacitance has nothing to do with load R_L, while in the other three topologies it is a function of the

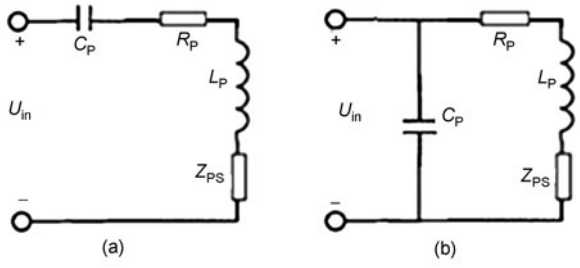

Figure 4 Equivalent primary circuit with reflected impedance. (a) Series compensated primary; (b) parallel compensated primary.

Table 1 Equivalent load impedance of WPT system

Series compensated primary	Parallel compensated primary
$1/(j\omega C_P) + R_P + Z_{PS} + j\omega L_P$	$1/(j\omega C_P)//(R_P + Z_{PS} + j\omega L_P)$

Table 2 Primary compensation capacitance C_P with ω_0

SS	SP	PS	PP
$\frac{1}{\omega_0^2 L_P}$	$\frac{R_S^2+2R_SR_L+\omega_0^2L_S^2}{\omega_0^2L_P(R_S^2+2R_SR_L+\omega_0^2L_S^2)-\omega_0^4M^2L_S}$	$\frac{L_P}{(R_P+\frac{(\omega M)^2}{R_S+R_L})^2+\omega_0^2L_P^2}$	$\frac{\omega_0L_P+\mathrm{Im}\,Z_{PS}}{\omega_0((R_P+\mathrm{Re}\,Z_{PS})^2+(\mathrm{Im}\,Z_{PS}+\omega_0L_P)^2)}$

load. Meanwhile as a power supply system, its load is of great randomness and it is impractical to allow the primary compensation capacitance C_P to vary with the load change. Then in this paper, a phase controlled inductor circuit is further presented to solve the issue of the primary compensation capacitance fluctuation with load change and to guarantee the flexible applications of all topologies.

4 Phase controlled inductor circuit design

In order to ensure the practical applications of various topologies, namely to solve the problem of C_P fluctuation with load change, a phase controlled inductor circuit is proposed to tune the system real-timely and dynamically as shown in Figure 5.

By controlling the switch of fully controlled electric components, the phase shift control of inductive current is realized to enable the parallel branch to fluctuate from capacitive to inductive successively. VT_1 and VT_2 are two fully controlled components in series with diode, anti-parallelly coupled. The VT_1 has a triggering angle of $180°> \alpha >90°$, and by lagging VT_1 180°, the VT_2 is triggered. Suppose $u=U\sin(\omega t)$, the output voltage waveform u_T of L_T is shown in Figure 6.

Usually the resistance R of inductive branch can be neglected because $\omega L_T \gg R$. In one period, the electric angles of the current and voltage of L_T are equal to 2π-2α and the voltage waveform is plus-minus half-wave symmetry. The inductor voltage can be expanded into a Fourier series, given as

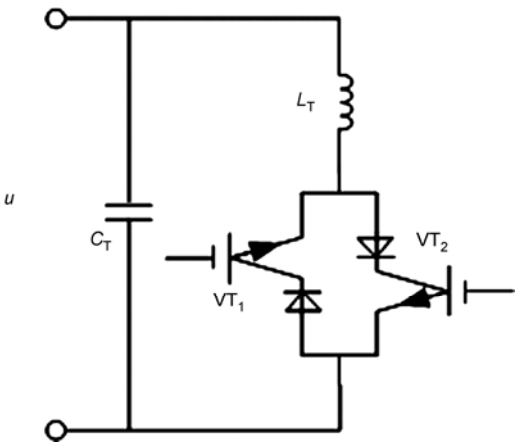

Figure 5 Phase controlled inductor circuit.

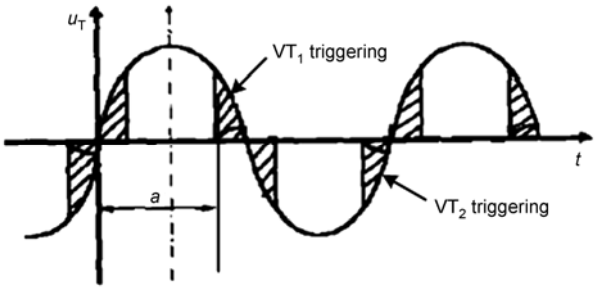

Figure 6 Voltage waveform of inductance L_T.

$$\begin{aligned} u_T &= \sum_{n=1,3,5\cdots}^{\infty}(a\cos n\omega t + b_n \sin n\omega t) \\ &= \frac{U}{\pi}(2\pi - 2\alpha + \sin 2\alpha)\cos\omega t \\ &\quad - \sum_{2K+1}^{\infty}\frac{2U}{\pi}\left(\frac{\sin(n+1)(\alpha-\pi/2)}{n+1}\right. \\ &\quad \left. + \frac{\sin(n-1)(\alpha-\pi/2)}{n-1}\right)\cos n\omega t. \end{aligned} \tag{7}$$

And the fundamental component is deduced as

$$u_{T1} = \frac{U}{\pi}(2\pi - 2\alpha + \sin 2\alpha)\cos(\omega t). \tag{8}$$

Then the equivalent inductance of the inductive branch is

$$L_{eq} = \frac{U}{\omega I} = \frac{\pi L_T}{2\pi - 2\alpha + \sin 2\alpha}. \tag{9}$$

The equivalent susceptance in parallel with C_T is

$$Y = j\left(\omega C_T - \frac{2\pi - 2\alpha + \sin 2\alpha}{\omega\pi L_T}\right). \tag{10}$$

When $\alpha=\pi$ and $Y=j\omega C_T$, the parallel branch is capacitive, while when $\alpha=\pi/2$ and if $\frac{1}{\omega L_T} > \omega C_T$, $Y = -j\left(\frac{1}{\omega L_T} - \omega C_T\right)$, it is inductive. As a result, by selecting appropriate capacitance and inductance, the phase controlled circuit can be used to make the parallel branch fluctuate between capacitive and inductive, and the equivalent susceptance is correlated with the triggering angle.

5 Dynamic tuning control

With the designed phase controlled inductor circuit, the

real-time tuning control to SP, PS and PP topologies can be achieved to guarantee their flexible practical applications, but with some differences in the specific control method.

5.1 Dynamic tuning control of SP topology

Paralleling the phase controlled inductor circuit with the secondary circuit of SP topology and merging C_S and C_T to C_{ST} for simplifying circuit, the dynamic tuning secondary circuit is shown in Figure 7.

In order to ensure the maximum transfer power, the system operating frequency is set at the resonance frequency ω_0. From Figure 7, the equivalent impedance (Z_{S0}) of the secondary circuit is deduced and given as

$$Z_{S0} = R_S + j\omega_0 L_S + \frac{1}{j\omega_0 C_{ST}} // j\omega_0 L_{eq} // R_L. \quad (11)$$

In eq. (11), it is evident that $\mathrm{Im}Z_{S0}$ is correlated with L_{eq} and C_{ST}. By selecting the reasonable L_T and C_{ST} of the dynamic tuning circuit and adjusting the triggering angle α, it is passable to make $\mathrm{Im}Z_{S0}$ equal to zero. Then based on the analysis in Section 4, the primary compensation capacitance C_P is consistent with SS topology, equal to $1/(\omega_0^2 L_P)$, and independent of the load resistance R_L. Therefore, the system operating frequency could be controlled at the resonance frequency of the secondary circuit by the phase controlled inductor circuit and the primary compensation capacitance is independent of load resistance.

At system work, we could detect the voltage and current of the secondary circuit and calculate the impedance angle θ and the corresponding triggering angle α to tune the system. However, it also has its limitations, since the reasonable parameters of the inductor circuit cannot be chosen randomly. Once the resonance frequency and these parameters are determinate, the system could be tuned only within the specific load range. By solving $\mathrm{Im}Z_{S0}=0$, the range of load resistance could be deduced

$$R_L \geqslant 2\omega L_S. \quad (12)$$

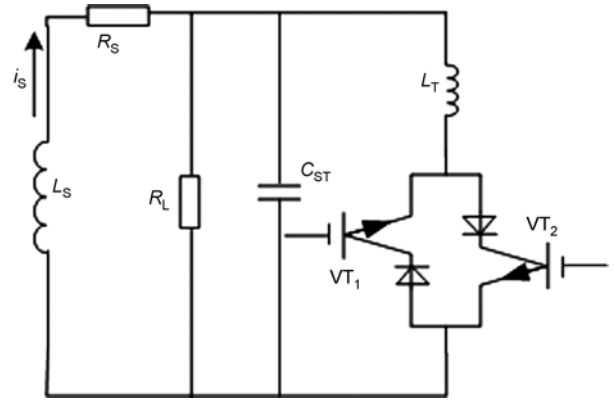

Figure 7 Dynamic tuning secondary circuit of SP topology.

5.2 Dynamic tuning control of PS or PP topology

Similarly, paralleling the phase controlled inductor circuit with the primary circuit of PS or PP topology and merging C_P and C_T to C_{PT}, the dynamic tuning primary circuit is shown in Figure 8.

From Figure 8, the equivalent impedance (Z_{in}) is deduced with the operating frequency ω_0, given as

$$Z_{in} = \frac{1}{j\omega_0 C_{PT}} // j\omega_0 L_{eq} // (R_P + j\omega_0 L_P + Z_{PS}). \quad (13)$$

In eq. (13), $\mathrm{Im}Z_{in}$ depends on L_{eq} and C_{PT}. So by selecting the reasonable L_T and C_{PT} and adjusting the triggering angle α, $\mathrm{Im}Z_{in}$ is liable to equate to zero. Then we need to detect the system input voltage U_{in} and the fundamental component of input current i_i to calculate the impedance angle θ and the corresponding triggering angle α to tune system and to maximize power transfer.

6 Simulation and experiment

Figure 9 shows the experimental setup for ICWPT system. In Figure 9, Colpitts oscillator is used to produce high frequency voltage signal with the angular frequency of 3.45 Mrad s^{-1}. Due to the series resonance adopted in the primary circuit, in this paper the simulation and experiment of dynamic tuning control are mainly carried out for the SP topology. The key system parameters are given in Table 3.

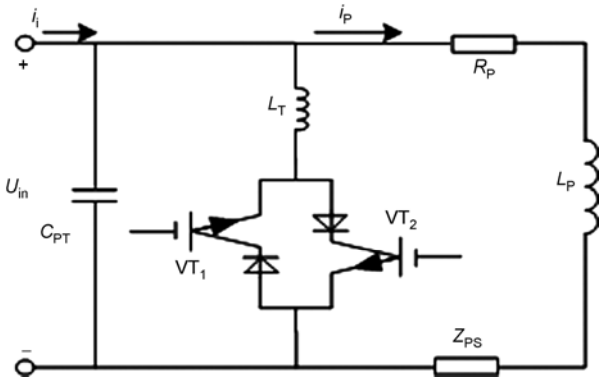

Figure 8 Dynamic tuning primary circuit of PS or PP topology.

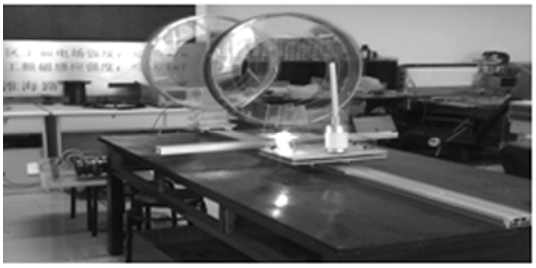

Figure 9 Prototype of experimental device.

Table 3 Parameters of experimental system

Turns	Radius	Inductance	Radiation resistance	Dynamic tuning circuit
N_P=N_S=5	r_P=r_S= 0.3 m	L_P=L_S= 7.12 μH	R_P=R_S= 0.36 Ω	L_T=10 μH, C_{ST}=9.73 pF

When load R_L is 100 Ω, the theoretical values (TV) and experimental values (EV) of η_{SS} and η_{SP} are shown in Figure 10. Where η_{SS} and η_{SP} stand for the transfer efficiencies of SS and SP topology respectively. However, it should be noted that the efficiency built on the transfer system, which is defined as the ratio of the output active power of the load to the input active power generated by the primary coil, does not include the high-frequency power supply system which is treated as a constant voltage source.

Clearly in Figure 10, when the transmission distance is less than 0.25 m, η_{SS} is slightly larger than η_{SP} and the SS topology should be selected to ensure a larger efficiency. If the distance is greater than 0.25 m or increases further, η_{SP} is much greater than η_{SS}. Then the SP topology should be adopted. Therefore, it is quite necessary to study the transfer capacity of various topologies and launch the experiment research of the PS and PP topologies.

When the distance D is 0.45 m and with the parameters shown in Table 3, the efficiency of the SP topology is greater. To achieve the maximum transfer efficiency, the C_P should be set appropriately. But for the SP topology, the C_P is varied with the load change. To solve this problem, a phase controlled inductor circuit is designed to tune the WPT system and the simulations and experiments of tuning SP topology are illustrated below.

Figure 11 shows the simulation results after tuning dynamically the SP topology by paralleling the phase controlled inductor circuit with the secondary circuit.

In Figure 11(b), when the load is 200 Ω, the triggering angle α is equal to 2.561 rad. While in Figure 11(a), when α is 2.562 rad, the impedance angle is -5.78×10^{-6} rad, approximately equal to zero. It indicates that when the secondary circuit is connected directly to a load of 200 Ω, we can adjust α

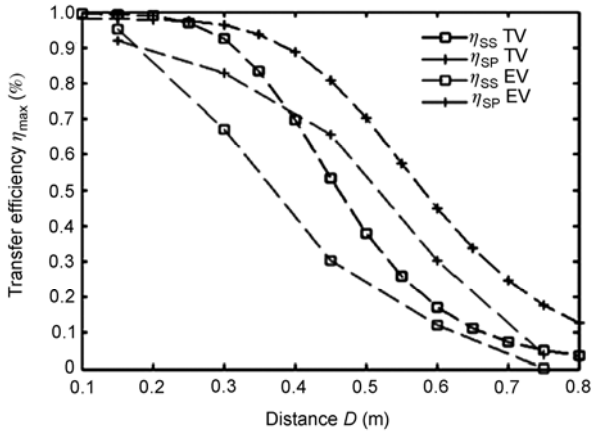

Figure 10 Transfer efficiency comparison of SS and SP topologies.

(2.561 rad) to make system resonance coupling and achieve the optimal transfer efficiency. It is consistent with the above theoretical analysis.

In HF, due to the difficulty of continuous resistance change regulation, only a few resistances between 100 Ω and 400 Ω are selected to verify the effectiveness of the proposed method in the experiments. The theoretical and experimental values of α are shown in Table 4 with the various load.

We can see from Table 4 that some discrepancies exist between the experimental and theoretical values. The main reasons lie in the neglect of high frequency radiate loss when the theoretical values are calculated, inaccuracy of system parameters got from manual coils and the different load resistances under different temperatures. Disregarding these factors, the experimental results are consistent with the theoretical values.

Figure 12 shows the voltage and current waveforms of the secondary coil with or without dynamic tuning phase controlled inductor circuit to tune the SP topology when R_L is 100 Ω.

In Figure 12(a), when R_L is 100 Ω and ω_0 is 3.45 Mrad s^{-1}, in the secondary coil the phase of the current lagging the voltage is about 13° and the active power transferred from

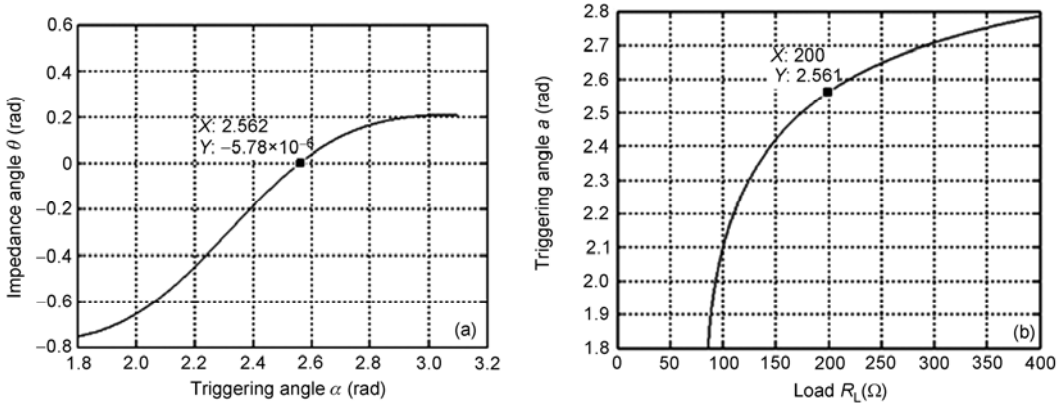

Figure 11 Simulation of dynamic tuning for the SP topology. (a) Curve of impedance angle θ varied with α when R_L=200 Ω; (b) curve of triggering angle α varied with R_L.

Table 4 Triggering angle α

Load R_L (Ω)	α (rad)	
	Theory	Experiment
100	2.097	2.181
150	2.419	2.500
200	2.561	2.601
250	2.648	2.796
300	2.707	2.830
350	2.751	2.875
400	2.786	2.850

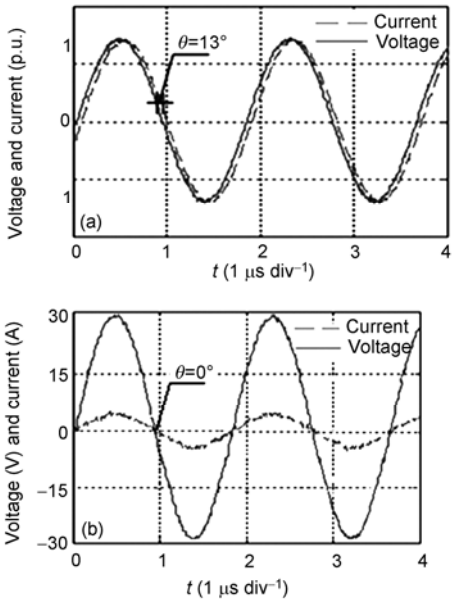

Figure 12 Voltage and current waveforms of the secondary coil when R_L is 100 Ω. (a) Voltage and current waveforms without dynamic tuning; (b) voltage and current waveforms with dynamic tuning.

the primary coil to the secondary coil is about 58 W, while the output active power of R_L is about 53 W. Due to the small phase, the voltage and the current are normalized for more obvious comparison. Then the secondary-to-primary reflected impedance is not pure resistance, needing to adjust C_P to keep system resonant. Paralleling the designed phase controlled inductor circuit can automatically tune the system and keep system zero phase angle operating by adjusting the triggering angle, as shown in Figure 12(b). Then the maximum power transfer is achieved, with about 67 W transfer power and 60 W output power, increasing by 15.5% and 13.21% respectively.

7 Conclusions

In this paper the maximum power transfer capability of four basic topologies and system dynamic tuning control by the designed phase controlled inductor circuit are investigated. By building and studying the equivalent circuits of four basic topologies in HF, the way of selecting the primary compensation capacitance C_P to ensure the maximum power transfer capability is proposed. Nevertheless, except SS topology, the compensation capacitances of the other three topologies fluctuate with load change, which is an obstacle to practical applications for the three topologies. To solve this problem, a phase controlled inductor circuit is further proposed. By paralleling the phase controlled inductor circuit with the secondary circuit of SP or the primary circuit of PS and PP, and adjusting the triggering angle, the WPT system could be dynamically tuned at zero phase angle frequency to maximize power transfer. Finally, simulations and experiments show that the proposed method is of effectiveness to solve the issue of resonance compensation capacitance fluctuation with the load change and to guarantee the flexible applications of all topologies.

The load studied in this paper is pure resistance load, but in practical application, it is likely to encounter non-pure resistive load, then the expression of C_P would become more complex. The proposed method of paralleling a phase controlled inductor circuit could also solve this problem, but whether there are some constraints similar to eq. (12) is a goal of our further work. Moreover, it is easy to find that C_P is also correlated with the mutual inductance M between coils, while M is inversely proportional to the three powers of transmission distance D [9]. Meanwhile once the distance D is changed, the C_P will change, leading to the bifurcation phenomenon and greatly weakening the power transfer capability. By adjusting the triggering angle, the presented dynamic tuning control method can stabilize the system operational frequency at the resonant frequency of the secondary circuit, while whether this method can avoid the bifurcation phenomenon is another goal of our future work.

This work was supported by the National High-Tech Research & Development Program of China ("863" Program) (Grant No. 2012AA050210), the National Natural Science Foundation of China (Grant No. 51177011), the Research Innovation Program for College Graduates of Jiangsu Province (Grant No. CXZZ11_0150) and Scholarship Award for Excellent Doctoral Student granted by Ministry of Education of China.

1 Tesla N. U.S. Patent 1119732, 1914
2 Boys J T, Green A W. Inductively coupled power transmission concept-design and application. IPENZ Trans, 1995, 22(1): 1–9
3 Manolatou C, Khan M J, Fan S H, et al. Coupling of modes analysis of resonant channel add-drop filters. IEEE J Quantum Electron, 1999, 35(9): 1322–1331
4 Hirai J J, Kim T W, Kawamura A. Wireless transmission of power and information for cableless linear motor drive. IEEE Trans Power Electron, 2000, 15(1): 21–27
5 Mandal T K. Wireless transmission of electricity development and possibility. In: Proceedings of Sixth international symposium Nikola Tesla. Belgrade, Serbia, October 18–20, 2006. 197–200
6 Soljačić M. Wireless energy transfer can potentially recharge laptops, cell phones without cords. Report in San Francisco Massachusetts Institute of Technology, 2006
7 Jang Y, Jovanovic M M. A contactless electrical energy transmission system for portable-telephone battery chargers. IEEE Trans Indus Electron, 2003, 50: 520–527

8 Hirai J J, Kim T W, Kawamura A. Wireless transmission of power and information for cableless linear motor drive. IEEE Trans Power Electron, 2000, 15(1): 21–27
9 Soljačić M, Kurs A, Karalis A, et al. Wireless power transfer via strongly coupled magnetic resonances. Sciencexpress, 2007, 112: 1–10
10 Fredy S, Jesús G C, Jordi S, et al. Wireless power of single-chisystems with integrated coil and external wire-loop resonator. Appl Phys Lett, 2008, 92(7): 074102 (1–3)
11 Imura T, Okabe H, Hori Y, et al. Basic experimental study on helical antennas of wireless power transfer for electric vehicles by using magnetic resonant couplings. In: Proceedings of Vehicle Power and Propulsion Conference, Dearborn, MI, 2009. 936–940
12 Zou Y W , Huang X L, Tan L L, et al. Current research situation and developing tendency about wireless power transmission. In: Proceedings of ICECE2010, Wuhan, China, 2010. 3507–3511
13 Tan L L, Huang X L, Li H, et al. Study of Wireless Power Transfer System Through Strongly Coupled Resonances. In: Proceedings ICECE2010, Wuhan, China, 2010. 4275–4278
14 Sample A P, Meyer D T, Smith J R. Analysis, experimental results, and range adaptation of magnetically coupled resonators for wireless power transfer. IEEE Trans Indus Electron, 2010, 99: 1–11
15 Tan L L, Huang X L, Huang H, et al. Transfer efficiency optimal control of magnetic resonance coupled system of wireless power transfer based on frequency control. Sci China Tech Sci. 2011, 54(6): 1428–1434
16 Yan G Z, Ye D D, Zan P, et al. Micro-robot for endoscope based on wireless power transfer. In: Proceedings of the 2007 IEEE international Conferrnce on Mechatronics and Automation. Harbin, China, August 5-8, 2007. 3577–3581
17 Jung K H, Kim Y H, Kim J, et al. Wireless power transmission for implantable devices using inductive component of closed magnetic circuit. Electron Lett, 2009, 45: 21–22
18 Fu W Z, Zhang B, Qiu D Y, et al. Maximum efficiency analysis and design of self-resonance coupling coils for wireless power transmission system. Proc CSEE,2009, 29(18): 21–26
19 Sedwick R J. Long rang inductive power transfer with superconducting oscillators. Ann Phys, 2010, 25:287–299
20 Wang C S, Covic G A, Stielau O H. Power transfer capability and bifurcation phenomena of loosely coupled inductive power transfer systems. IEEE Trans Indus Electron, 2004, 51: 148–157
21 Zhou W Q, Ma H, He X N. Investigation on different compensation topologies in inductively coupled power transfer system. Trans China Electrotech Soc, 2009, 24(1): 133–139
22 Qiang H, Huang X L, Tan L L, et al. Study on topology design of wireless power transfer for electric vehicle based on magnetic resonance coupling. Adv Mater Res, 2011, 308-310: 1000–1003